Improving rapeseed carbon footprint evaluation via the integration of remote sensing technology into an LCA approach: A case study in Southwest China

Xueqing Yang[a,b,1], Xiuchun Dong[a], Alberto Bezama[b], Yang Liu[c,*]

[a] Institute of Remote Sensing and Digital Agriculture (Chengdu Agricultural Remote Sensing Sub-center), Sichuan Academy of Agricultural Sciences, Chengdu, China

[b] Department of Bioenergy, Helmholtz-Centre for Environmental Research (UFZ), Leipzig, Germany

[c] Chair of Management, Innovation and Sustainable Business, University of Augsburg, Augsburg, Germany

Abstract:

Agricultural carbon footprint (CF) evaluation plays an important role in climate change mitigation and national food security. Many studies have been conducted worldwide to evaluate the CF of rapeseed and its byproducts; however, only few of these studies have considered finer-scale spatial-temporal heterogeneity at the regional scale. Considering the superiority of the use of detailed crop information extracted by remote sensing (RS) techniques, we attempted to integrate RS into life cycle assessments to improve rapeseed CF evaluation. The results of our case study suggest that (1) the proposed approach is applicable for high-resolution (10 m *10 m) rapeseed distribution mapping in Southwest China and that (2) the farm-based CFs (FCFs) of rapeseed in the studied region range from 3,333.08 to 4,572.82 kgCO_2-eq ha^{-1}, while the product-based CFs (PCFs) vary from 1,316.23 to 2,443.95 kgCO_2-eq t^{-1}. Nitrogen fertilizer processing and its application are identified as the dominant

[1] Corresponding authors: Xueqing Yang, xueqing.yang@ufz.de and Yang Liu, yang1.liu@uni-a.de.

contributors to upstream and downstream greenhouse emissions (GHGs), respectively. (3) The significant role of soil properties and soil organic carbon in influencing crop PCFs indicates good GHG offsets. The method used in the current study has strong adaptability and universality in different areas with various climatic conditions and can provide a solid basis for policymakers to formulate differentiated agricultural carbon reduction policies.

Keywords: Remote sensing, Carbon footprint, Rapeseed production system, Life cycle assessment, Soil organic carbon, Greenhous gas emission

1. Introduction

Climate change is, by far, the greatest challenge that human society has faced together (Rosenzweig et al., 2020). Among the different sectors, global food systems contribute approximately one-third of global anthropogenic greenhouse gas (GHG) emissions (Menegat et al., 2022). In the face of both climate change and food security issues caused by population expansion, increasing agricultural production efficiency from the perspective of decreasing GHG emissions is urgent (Zhang et al., 2021). To achieve this goal, the quantification of the GHG emissions of entire crop production systems plays a crucial role in identifying emission hotspots and further improving carbon emission performance (Tian et al., 2021; Liu et al., 2022; Feng et al., 2023).

The carbon footprint (CF) is an effective indicator for calculating carbon emissions in a product system with a specific system boundary, and is expressed as CO_2 equivalents (CO2-eq) (ISO14067, 2013). The whole life cycle of agricultural production activities includes the substances and agricultural inputs comsumption, planting management, harvesting and transportation, and waste recycling (Boettcher et al., 2020). Depending on the system boundary, the life cycle assessment (LCA) approach is adopted to quantify the environmental impacts of products ranging from “cradle to grave”, “cradle to gate” and “gate to grave”. However, the quality of the classic LCA results highly depends on accessible inventories, which are normally aggregated or averaged conditions at a higher level, and thus have poor spatial and temporal resolution (Reap et al., 2008). To cope with this, there is an emerging trend to improve the spatial and temporal heterogeneity of LCA by integrating geographic information systems (GISs) (Gasol et al., 2011; O'Keeffe et al., 2016b; Escobara et al., 2020; Yang et al., 2022) or coupling with process-based models for better simulation of the carbon nitrogen cycle, such as DNDC (DeNitrification-DeComposition) (Tabatabaie et al., 2018; Medel-Jiménez et al., 2022; Medel-Jiménez et al. 2024), NUFER (NUtrient flows in Food chains, Environment and Resources use) (Guo et al., 2022), Candy (CArbon and Nitrogen DYnamics) (O'Keeffe et al., 2016b) and so forth. Nevertheless, due to the complex nature of crop growth, variations in regional management strategies and local economic development levels, the CF results are still regarded with great uncertainty (Finnveden, 2000; Hellweg and Milà, 2014).

Rapeseed (*Brassica napus L.*) is widely cultivated as an important biomass energy source in Europe, and is considered as the major edible oil crop and ornamental and economic crop in China (Yang et al., 2022). Chinese rapeseed can be divided into spring- and winter- rapeseed varieties, which have different phenological calendars both spatially and temporally. The winter rapeseed is dominant in Southwest China, and is mainly distributed in the lower reaches of the Yangtze River (LYRB), including Yunnan, Guizhou, and Sichuan provinces and Chongqing municipality. This region is dominated by smallholder-owned agricultural land, which has complex agricultural planting structures, small-scale agricultural systems and diverse agricultural management methods, leading to additional difficulties in mitigating CO_2 emissions. Referring to GHG emission evaluation, existing studies offer certain insights into the CF of rapeseed production at the national level. As documented in previous studies, the CF of rapeseed during production ranges from 1.45 to 2.26 t CO_2-eq ha^{-1} in various regions of China (Wang et al., 2019; Guo et al., 2022). Among the four rapeseed production subregions in China, the highest CF was observed in the LYRB, which also has the highest N application rate (Guo et al., 2022). Farm surveys, agricultural statistics or estimated data were adopted in these studies; however, the average value estimated for each province is obviously too coarse to discuss the spatial pattern of CFs at the regional- scale. Moreover, the comprehensiveness and objectiveness of farm surveys are easily influenced by the quality of farmers' feedback, and large-scale surveys cannot always be guaranteed when considering workload. Thus, the existing studies failed to underpin a useful strategy that guarantees finer spatial-temporal information on rapeseed CF in Southwestern China.

Remote sensing (RS) technology has the obvious advantages of objectivity, efficiency, cost and large-scale synchronous observation. In particular, RS can obtain key biophysical and chemical parameters related to rapeseed production, providing reliable input data and spatial distribution patterns for crop growth models, data assimilation systems and yield estimations. There are already successful rapeseed mapping studies, which can be categorized as empirical index-based, machine learning-based and hybrid methods. Nevertheless, there are no golden-rules for choosing the best method, as they inevitably have their respective advantages and limitations. For instance, the empirical index-based method is commonly based on the spectral features of the rapeseed flowering period, which is straightforward to implement. Representative examples include the Canola index (CI) (Ashourloo et al., 2019), normalized difference vegetation index (NDVI) (Han et al., 2021a), enhanced vegetation index (EVI) (Tao et al., 2020) and enhanced area yellow index (EAYI) (Zeng et al., 2020). However, these phenology-based rapeseed mapping methods rely heavily on images of flowering periods, and are easily disturbed by cloud noise (Zeng et al., 2020). Machine learning-based approaches, such as artificial neural networks (ANNs) (Tao et al., 2019) and random forest regression (RFR) (Meng et al., 2020), can overcome this problem by learning nonflowering features from training samples for rapeseed mapping. Unfortunately, machine learning-based approaches require large training sample, and sample collection and validation are usually time-consuming and labour-intensive. The hybrid approach combines the advantages of both empirical index-based and machine-learning methods, such as seamless and automated rapeseed mapping (SARM) (Zhang et al., 2022) and rule-based sample generation and a one-class classifier (RSG-OC) (Zang et al., 2023). Regrettably, the limitations of applying SARM to large-scale and long-term rapeseed mapping in complex cultivation systems are obvious that due to the inability of the winter rapeseed index to distinguish rapeseed from other non-rapeseed classes. Additionally, the application of RSG-OC in regions of Southwest China displayed relatively poorer performance due to the difficulty of capturing flowering stage from cloud noise.

To address the abovementioned issues, in this study we attempted to (1) generate finer-resolution rapeseed distribution maps via the RS technique in regions of Southwest China; (2) assess the product carbon footprint (PCF) and farm carbon footprint (FCF) of rapeseed production; (3) and analyse the GHG emission hotspots in the studied region and their environmental and socioeconomic effects. To our knowledge, this is the first study in which RS is integrated into LCA for improving rapeseed CF evaluation; we consider this a promising way to solve the common challenges faced by agricultural CF assessments and address the practical demand for more detailed crop information in this region. The method used in the current study has strong adaptability and universality in different areas with various climatic conditions and can provide a solid basis for policymakers to formulate differentiated agricultural carbon reduction policies.

2. Materials and methods

2.1 General information on the study region

The Chengdu Plain is located in the centre of Sichuan Province and covers a total area of 18,810.00 km^2; it consists of six cities: Meishan, Leshan, Chengdu, Mianyang, Yaan and Deyang, as shown in Fig. 1a. This plain is one of the most important grain- and rapeseed-producing areas in China and has been known as the “Tianfu Granary” since ancient times. As the largest plain in Southwest China, the Chengdu Plain has diverse environmental and climatic conditions. The elevation ranges from 248.00 to 5,694.00 m above sea level, as illustrated in Figure 1b. The Chengdu Plain belongs to the warm and humid subtropical southeast monsoon climate zone of the Pacific Ocean, and the annual average temperature and precipitation are 16.10°C and 929.40 mm, respectively. The soil types on the plain are mainly paddy soil and purple soil. The cultivation system, rather than animal husbandry, serves as the major income source for the local people. In the paddy rice-dryland crop rotation system, the dominant dryland crops are wheat, rapeseed, vegetables and orchards.

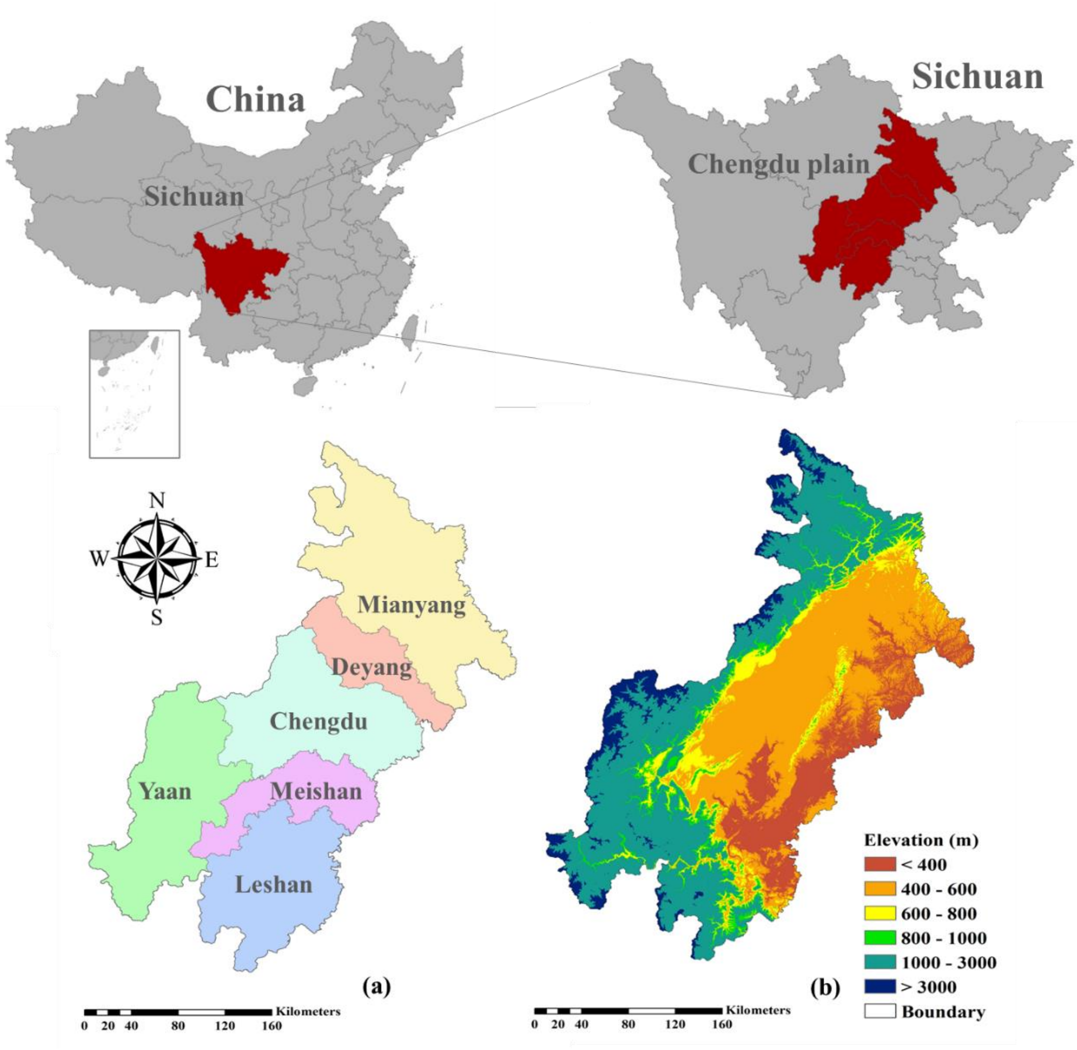

Figure 1. The geographic location of the study site: a) municipal units and b) elevations above sea level.

2.2 Agricultural data

We chose the city level as the primary spatial scale for collecting the main agricultural data; at this level, the finest and most complete data could be obtained. The main agricultural crop production data on sowing area, yield, fertilizer application, irrigation, and agronomic machinery application were collected for each studied city in 2021, namely, Meishan, Leshan, Chengdu, Mianyang, Yaan and Deyang, as displayed in Fig. 1a. Additional rapeseed fertilizer was obtained from the National Agricultural Products Input Summary (Appendix, Table S.1).

2.3 RS-based crop mapping information

2.3.1 Rapeseed mapping based on optical and SAR characteristics

We collected RS images of the Chengdu Plain from the Sentinel-2 (S-2) and Sentinel-1 (S-1) satellites launched by the European Space Agency. The S-1/2 imagers were collected during the dominant flowering season of rapeseed from March 5th to 20th, 2021. Due to differences in crop rotation (rice and rapeseed) and management practices, there are significant differences in the flowering period of rapeseed between Deyang and Mianyang, while in other rapeseed growth regions, the flowering periods are mainly concentrated around March 10th. Using 2021 as the baseline, we obtained red (b4), green (b3) and blue (b2) spectral bands with 10 m spatial resolution top-of-atmosphere (TOA) reflectance observations based on S-1/2 satellite images. The quality assessment band of the S2 TOA product was adopted to remove poor-quality images, such as severe cloud-obscured images. Then, we followed the approach proposed by Han et al. (2021) to use both optical and SAR features to identify rapeseed flowering and pod periods. The normalized difference yellow index (NDYI), which can capture increasing yellowness in a time series during the flowering period of rapeseed, is calculated as follows (Han et al., 2021b):

$$NDYI = \frac{green - blue}{green + blue} \quad (1)$$

The ground truth data were further collected for the same region in 2021 from the time of rapeseed flowering until the pod season. In total, 101 rapeseed ground truth points were obtained. According to the rapeseed sample data, we assigned different thresholds for regions to further conduct RS classification and extraction. The classification results were obtained by overlaying RS images to remove small patches, so we were able to construct a standardized distribution map of rapeseed plants on the Chengdu Plain.

2.3.2 Assessment of the accuracy of rapeseed classification

To ensure accuracy, the rapeseed areas derived from RS images were further compared with the data from statistical books, and the total area of rapeseed distribution in each city of the Chengdu Plain was compared with the baseline 2021 regional statistics. We used the RMSE, MAE and coefficient of determination (R^2) to quantify the classification accuracy (Eqs. (2) - (4)). These three indicators are constructed as follows:

$$RMSE = \sqrt{\sum_{i=1}^{n} \frac{(y_i - f_i)^2}{n}} \quad (2)$$

$$MAE = \frac{1}{n}\sum_{i=1}^{n} |y_i - f_i| \quad (3)$$

$$R^2 = \frac{\left(\sum_{i=1}^{n}(y_i - \bar{y_i})(f_i - \bar{f_i})\right)^2}{\sum_{i=1}^{n}(y_i - \bar{y_i})^2 \sum_{i=1}^{n}\left(f_i - \bar{f_i}\right)^2} \quad (4)$$

In addition, we used 416 ground truth points from the field sample to overlay with the created rapeseed distribution map to generate the confusion matrix and calculate the kappa index. By doing so, the classification consistency was evaluated. The main methodology framework is shown in Figure 2.

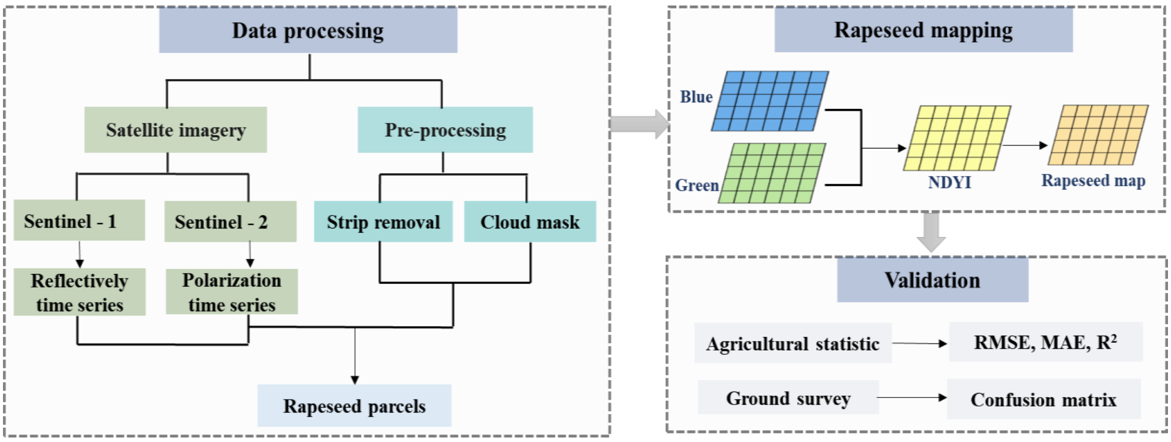

Figure 2. Workflow of rapeseed mapping by applying the NDYI and its accuracy test methodology

2.4 Carbon footprint evaluation

2.4.1 System boundary and functional unit of an LCA

In the present study, we set the system boundary from the cradle to the farm gate. The system boundary included both the background system and foreground system, as illustrated in Figure 3. Upstream emissions are released from the production of agronomic input materials, and downstream emissions are generated during field operations, such as sowing, irrigation, fertilization, harvesting and transportation. Other downstream processes, such as rapeseed oil production, transport, and consumption, were not considered in this study. We used yield-scaled GHG emissions, i.e., the product carbon footprint (PCF, kg CO_2-eq t^{-1}), and area-scaled GHG emissions, namely, the farm carbon footprint (FCF, kg CO_2-eq ha^{-1}), to evaluate the CF during rapeseed cultivation.

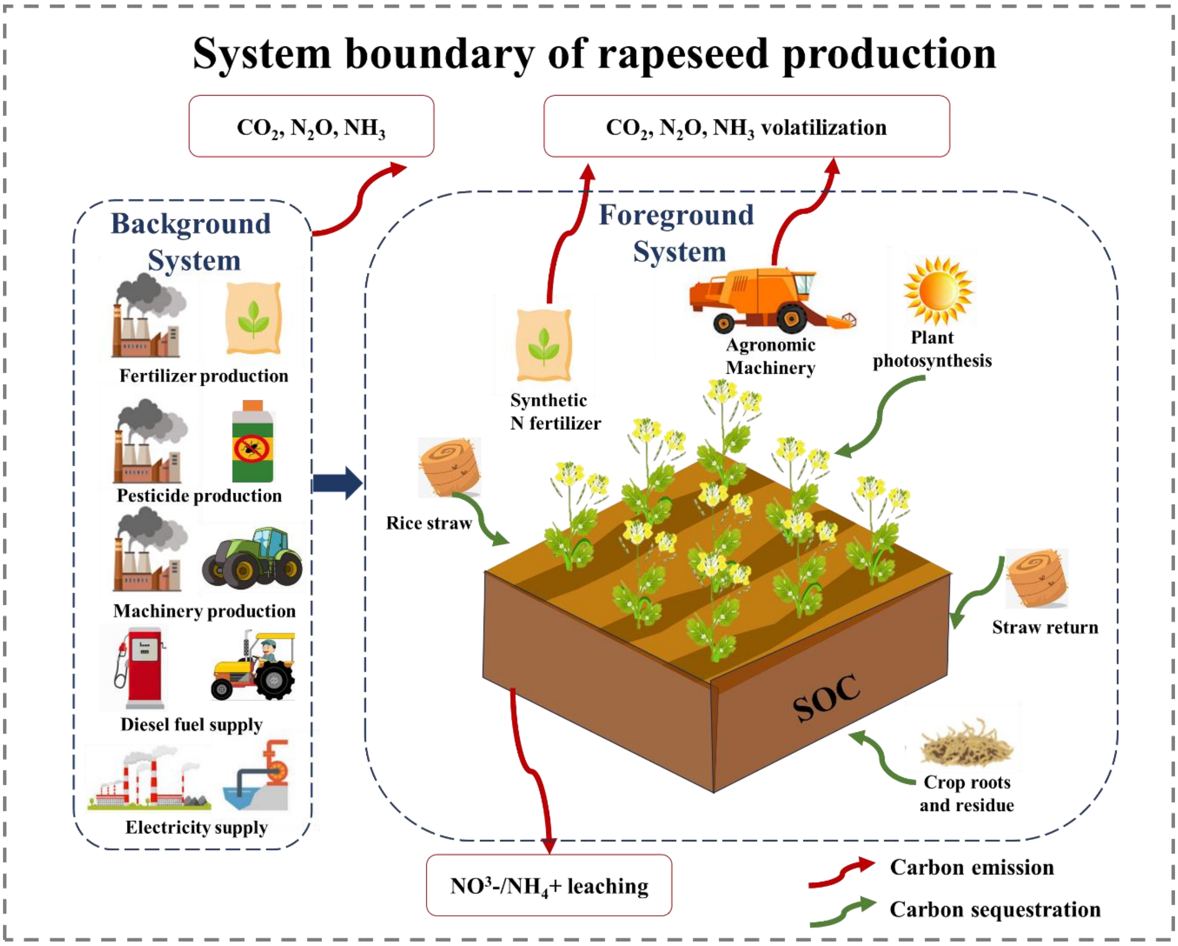

Figure 3. The system boundary set in the current study

2.4.2 GHG emission calculation

The GHG emissions during rapeseed production include both indirect and direct emissions. The indirect carbon emissions from rapeseed production systems include carbon emitted from the use of electricity, diesel oil, crop protection chemicals and other materials. The indirect emissions were calculated by summing the emissions from each agricultural input and multiplying by its emission coefficient via Eq. (5). The agricultural inputs in each system are illustrated in Figure 3, and their corresponding carbon emission coefficients are listed in Appendix, Table S.2.

$$CE_{i,CO_2} = \sum_j^i (AM_{i,j} \times EF_j) \quad (5)$$

Where $CE_{i,CO2}$ represents the sum of the emissions induced by the annual input of the j^{th} AM in kg CO_2-eq ha^{-1} yr^{-1}, where i and j are the respective crop and agricultural material amounts, respectively, and EF_j is the CO_2 emission factor of the corresponding AM_j.

The direct and indirect N_2O emissions from in-field nitrogen (N) fertilizer application were estimated using the following equation (IPCC, 2019):

$$CE_{i,N_2O} = N_2O_{i,D} + N_2O_{i,IN} = \{C_N \times (EF_{C-N2O} + EF_{C-NH3} \times 0.01 + EF_{RL} \times 0.0075)\} \times \frac{44}{28} \times 265 \quad (6)$$

where $CE_{i,N2O}$ represents the direct and indirect N_2O emissions from the application of chemical N fertilizer in kg CO_2-eq ha^{-1}. C_N is the quantity of N in chemical fertilizer applied during the annual production season (kg ha^{-1}). EF_{C-N2O} (= 0.01), EF_{C-NH3} (= 0.1) and EF_{RL} (= 0.3) represent the default emission factors of N_2O, NH_3 and NO_3^- runoff and leaching from chemical N fertilizer application, respectively; 44/28 is the molecular conversion factor of N_2 to N_2O; and 265 is the global warming potential of N_2O for the 100-year period (IPCC, 2014). The values 0.0100 and 0.0075 are the conversion coefficients of NH_3 volatilization and NO_3^- runoff and leaching in N_2O equivalents, respectively (IPCC, 2006).

Carbon sequestration by crop production systems includes carbon absorption by plants and soil organic carbon (SOC) due to straw and root residue return. Other sources, such as manure application and non-tillage management, were not considered in the present study. Normally, plant-absorbed carbon is harvested after growth. Thus, the change in SOC (ΔSOC, unit kg CO_2-eq yr^{-1}) during rice-rapeseed rotation was calculated as follows (Chen et al., 2021):

$$\Delta SOC_i = (SOC_{t1} - SOC_{t2}) \times \frac{44}{12} \quad (7)$$

$$SOC_{t1} = \frac{SR_{t1,i} + RB_{t1,i}}{1000} \times 29.025 + 272.33 \quad (8)$$

$$SOC_{t2} = \frac{SR_{t2,i} + RB_{t2,i}}{1000} \times 29.025 + 272.33 \quad (9)$$

$$SR_i = Y_i \times RSY_i \times PSR_i \quad (10)$$

$$RB_i = \frac{SR_i + Y_i}{RAR_i} \quad (11)$$

where SOC_{t1} and SOC_{t2} represent the soil organic carbon in the pre-rapeseed crop, namely, rice, and in rapeseed production, respectively. SR_i and RB_i represent the amount of crop straw and biomass of the root residue returned to the soil, respectively. Y_i represents the yield of the crop in dry weight (kg ha^{-1}). RSY_i represents the ratio of straw to yield (Zhang et al., 2010), and PSR_i is the proportion of straw return to the total biomass, which is calculated using the conversion of the harvest index of the crop, i.e., 0.3 (Peng et al., 2023). RAR_i refers to the ratio of aboveground biomass to root biomass (IPCC, 2019). The value 44/12 is the molecular conversion factor of *C* to CO_2.

The net carbon emissions (NCE_i, in kg CO_2-eq ha^{-1} yr^{-1}) of rapeseed were calculated as the difference between the total carbon emissions (TCE) and ΔSOC using Eqs. (12)-(13). The yield-scaled GHG emissions of rapeseed (PCF) were calculated as the net carbon emissions divided by the yield (Y_i) of rapeseed relative to the dry weight (Eq. (14)). The farm/area-scaled GHG emissions of rapeseed (FCFs) were computed by the net carbon emissions divided by the cultivation area (A) of rapeseed, as illustrated in Eq. (15).

$$TCE_i = CE_{i,CO2} + CE_{i,N20} \quad (12)$$

$$NCE_i = TCE_i - \Delta SOC_i \quad (13)$$

$$PCF_i = NCE_i / Y_i \quad (14)$$

$$FCF_i = NCE_i / A \qquad (15)$$

2.5 Pixel-level rapeseed yield map for PCF estimation and its influencing environmental and socioeconomic factors

The rapeseed FCF and PCF values were upscaled to the per-pixel level (10 m * 10 m) via integration into the rapeseed map. We could only access published statistical records, which have relatively coarse resolutions up to the city level. Moreover, it is known that the importance of rapeseed yield for calculating PCF and yield could be a good indicator of rapeseed genotype, growth environment and management strategies with high spatial heterogeneity. Thus, we conducted a rapeseed yield survey at the township level in the Chengdu Plain from 2022-2023 by interviewing village leaders and farmers. In total, 980-point specific yield information was collected and further used to interpolate the Chengdu Plain rapeseed yield map (Appendix, Figure S.1). The inverse distance weight (IDW) interpolation method of the "Interpolation analysis" toolbox in GIS was applied. Then, the interpolated yield map was overlayed with the rapeseed distribution map to skip the non-rapeseed area. The new PCFs of rapeseed can be updated by dividing the FCFs by the surveyed grain yield data. To clarify the driving factors of GHG emissions during rapeseed production, principal component analysis (PCA) was conducted to analyse the relationships of PCFs with environmental and socioeconomic factors. The environmental and socioeconomic influential factors were adopted and revised from Tian et al. (2021). All the factors considered were analysed by ArcMap 10.2 in raster format. Pearson's correlation test was employed to detect factors with high multicollinearity. Only one factor was retained for further PCA if two significantly correlated factors were identified. The detailed information on the influential factors is listed in Appendix, Table S.3.

3. Results

3.1 Rapeseed mapping based on the RS approach

Based on the workflow of mapping rapeseed areas, as displayed in Fig. 2, in the first step, we determined the threshold of the feature indicators. The imagery showed that the majority of the rapeseed pixels had the following values: red > 0.21, green > 0.24 and NDYI > 0.09. In the second step, we identified all rapeseed pixels from different images during the flowering period and subsequently aggregated them into annual rapeseed planting areas. To avoid misclassification due to poor-quality observations, we aggregated all the results classified from available S2 images to create a multitemporal dataset, which was assumed to have better performance. In the third stage, we combined the optical data with the SAR images to ensure the accuracy of the rapeseed maps. In the last step, we removed the "salt and pepper" noise by applying the threshold defined based on the number of connected objects and then filled the gaps inside the parcels. The output map is shown in Figure 4.

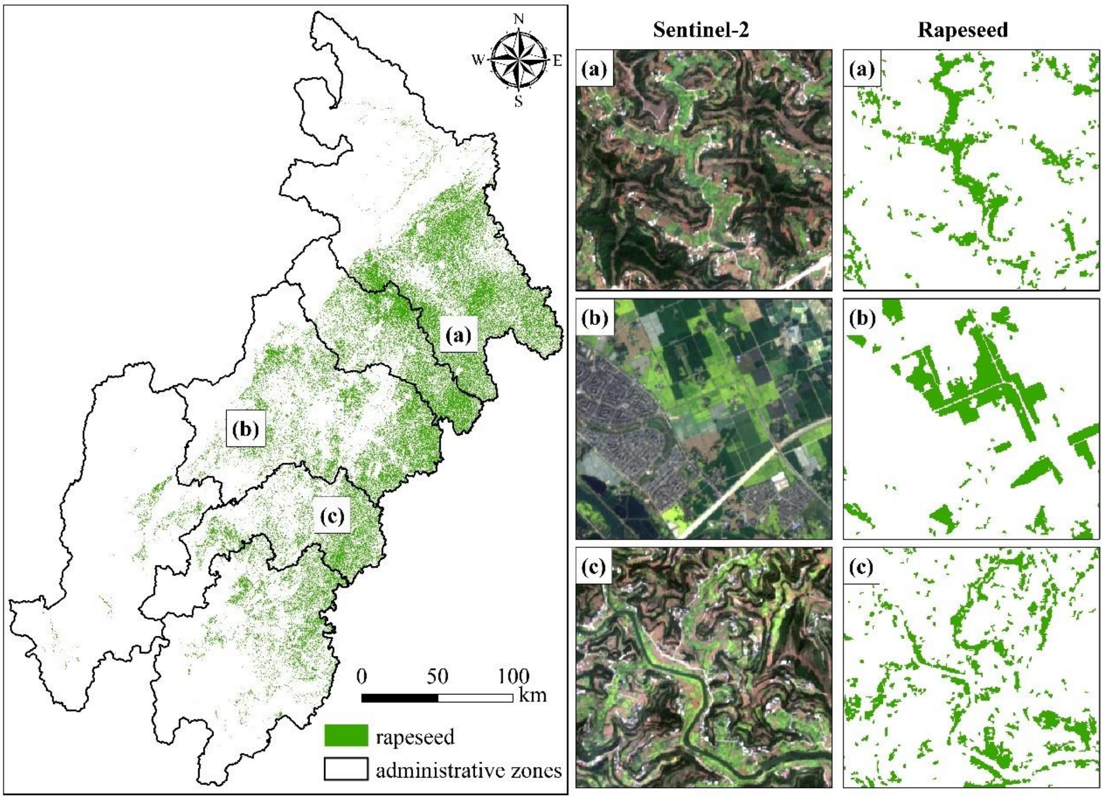

Figure 4. The rapeseed distribution map and three regions (a and c are mountainous areas, b is a plain area) demonstrating the spatial heterogeneity of the rapeseed field patches

3.2 Assessment of the mapping accuracy of the rapeseed

According to comparisons with regional agricultural statistics records, the identified cultivation area of rapeseed was smaller than the reported area. As illustrated in Appendix, Figure S.2, the RMSE, MAE and R^2 were 47,418.00 ha, 39,603.00 ha, and 0.8409, respectively. In addition, the RMSE and MAE accounted for less than 10% of the statistically reported rapeseed area. As illustrated in Appendix, Figure S.3, rapeseed cultivated in mountainous and plain areas exhibited significantly different patterns. The complexity of topographic conditions together with local agricultural management strongly affected the classification accuracy. After testing the rapeseed map with 416 ground truth points, a confusion matrix was generated, as reported in Appendix, Table S.4. The calculated kappa value was 0.7860, which represents good consistency with the classified rapeseed distribution map.

3.3 Spatial variation in GHG emissions from rapeseed production

We found large regional variations in GHG emissions from rapeseed production on the Chengdu Plain. As indicated in Figure 5 and Table 1, the FCFs of rapeseed on the Chengdu Plain ranged from 3,333.08 to 4,572.82 $kgCO_2$-eq ha^{-1}, with an average value of 3,892.25 $kgCO_2$-eq ha^{-1}. The rapeseed PCF varied from 1,316.23 to 2,443.95 $kgCO_2$-eq t^{-1}, with an average value of 170.18 $kgCO_2$-eq t^{-1}. N fertilizer processing accounted for approximately 43.09 - 66.52% of the upstream emissions, while the other main contributors were electricity usage (10.13 - 33.00%), NPK fertilizer production (7.57 - 20.90%) and diesel fuel production (1.11 - 20.37%). The dominant emission within downstream carbon emissions was the direct N_2O emission caused by N fertilizer application, which accounted for approximately 75.47%. A negative SOC change indicates soil carbon sequestration during rice-rapeseed rotation.

The spatial patterns of rapeseed FCFs and PCFs are displayed at the city level (Figure 6a and b) and at the pixel level (Figure 6c and d), respectively. Although the rapeseed cultivation area in Ya'an comprises only approximately 5.00 - 16.00% of the areas in the other five cities, it had the highest FCF and PCF values among all the studied areas on the Chengdu Plain. The main reason is that, from our point of view, the highest net carbon emissions in Ya'an resulted from the field N_2O emissions caused by intensive N fertilizer input. According to regional agricultural statistics, the yields of rapeseed from the highest to the lowest are as follows: Deyang (2,891.00 kg ha^{-1}), Mianyang (2,572.26 kg ha^{-1}), Chengdu (2,532.30 kg ha^{-1}), Meishan (2,162.02 kg ha^{-1}), Ya'an (1,871.08 kg ha^{-1}) and Leshan (1,752.81 kg ha^{-1}). Thus, the PCF values indicated that carbon hotspots were distributed in Leshan and Yaan, while other higher yield cities had relatively lower PCF values.

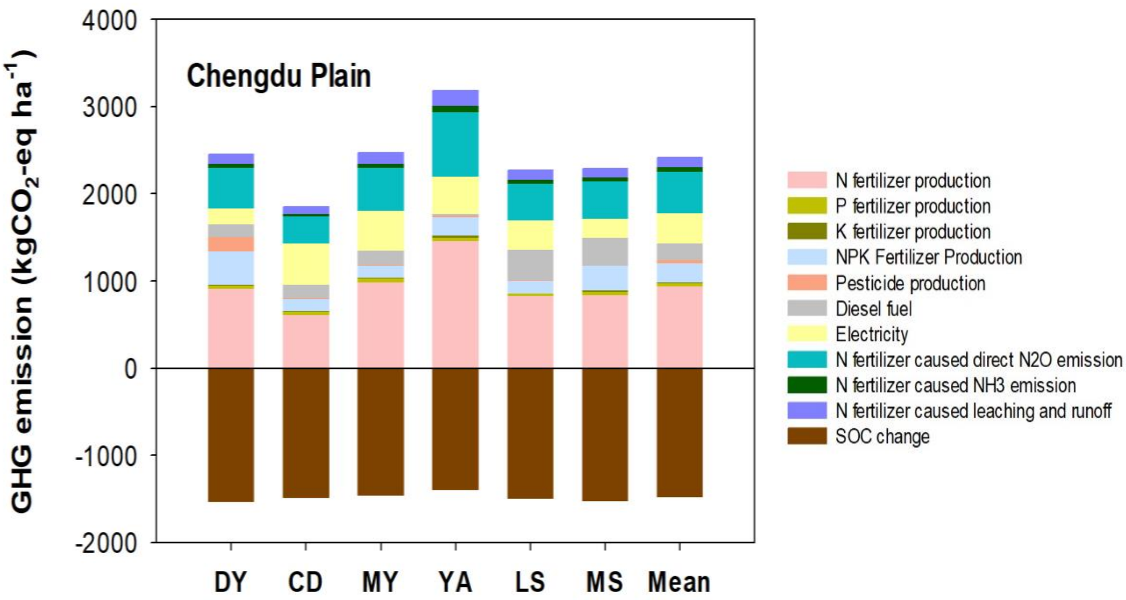

Figure 5. GHG emissions and key components in different regions of the Chengdu Plain.

Table 1. The GHG emissions from agricultural inputs for various regions of the Chengdu Plain in 2020.

Upstream carbon emission								Downstream carbon emission			Downstream carbon Sequestration	PCF	PCF
Region	N fertilizer	P fertilizer	K fertilizer	NPK Fertilizer	Pesticide	Diesel fuel	Electricity	Direct N_2O emission	NH_3 emission	Leaching and runoff	SOC change	FCF	PCF
	($kgCO_2$-eq ha^{-1} yr^{-1})												($kgCO_2$-eq t^{-1} yr^{-1})
MY	917.43	33.80	9.44	384.65	165.80	142.91	186.41	460.29	46.03	103.57	-1524.78	3975.09	1374.988
%	49.85	1.84	0.51	20.90	9.01	7.77	10.13	75.47	7.55	16.98			
DY	618.80	32.60	13.33	137.55	5.98	153.81	473.82	310.46	31.05	69.85	-1485.83	3333.082	1316.229
%	43.09	2.27	0.93	9.58	0.42	10.71	33.00	75.47	7.55	16.98			
CD	985.83	54.15	8.16	136.93	4.65	165.86	453.86	494.61	49.46	111.29	-1453.78	3918.589	1523.404
%	54.48	2.99	0.45	7.57	0.26	9.17	25.08	75.47	7.55	16.98			
YA	1466.42	36.02	24.64	210.43	16.36	24.46	426.00	735.73	73.57	165.54	-1393.64	4572.819	2443.948
%	66.52	1.63	1.12	9.55	0.74	1.11	19.33	75.47	7.55	16.98			
MS	838.92	22.28	5.39	146.54	7.62	347.43	337.52	420.91	42.09	94.70	-1495.08	3758.49	2144.271
%	49.18	1.31	0.32	8.59	0.45	20.37	19.79	75.47	7.55	16.98			
LS	844.75	33.17	22.68	276.74	7.92	312.46	226.67	423.83	42.38	95.36	-1515.46	3801.417	1758.27
%	48.99	1.92	1.32	16.05	0.46	18.12	13.14	75.47	7.55	16.98			
Mean	945.36	35.34	13.94	215.47	34.72	191.16	350.71	474.31	47.43	106.72	-1478.10	3893.248	1760.185
%	52.91	1.98	0.78	12.06	1.94	10.70	19.63	75.47	7.55	16.98			

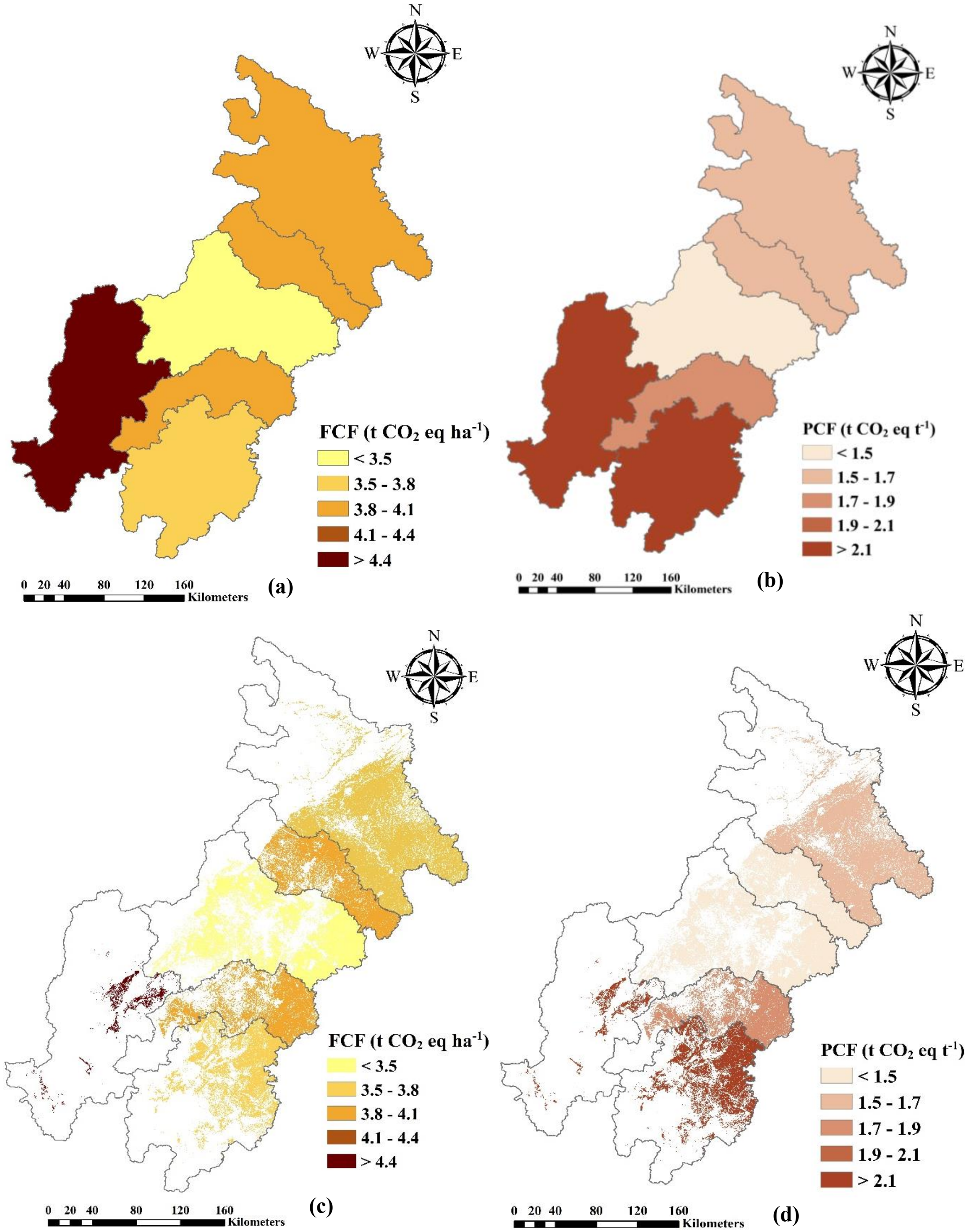

Figure 6 The spatial patterns of rapeseed FCFs (a, b) and PCFs (c, d) at the city and pixel levels, respectively

3.4 Main contributors to GHG emissions during rapeseed production

The rapeseed yield map generated by the GIS-based approach is displayed in Appendix, Figure S.4a. The surveyed grain yield ranged from 1.30 -5.20 t ha^{-1}, with an average value of 2.30 t ha^{-1}, while regional agricultural static yield ranged from 2.60 - 3.10 t ha$^{-1,}$ with an average yield of 2.10 t ha$^{-1,}$ on the Chengdu Plain. The geographic location of the PCF hotspots (Appendix, Figure S.4b) was consistent with the low rapeseed yield area (Appendix, Figure S.4a). Based on the Pearson correlation test results reported in Appendix., Figure S.5 and Table S.5, we excluded variables with high correlations, namely, those with correlation coefficients greater than 0.65 with other variables, to avoid multicollinearity in our subsequent analysis. The remaining eight variables were per capita GDP (*CapGDP*), total agronomic machinery power (*Machinery*), topsoil silt fraction (*Sand*), topsoil clay fraction (*Clay*), topsoil organic carbon (*SOC*), topsoil PH (*PH*), elevation above sea level (*Altitude*) and Rapeseed yield (*Yield*) (Appendix, Table S.6). The PCA results shown in Figure 7 revealed that the first and second principal components explained 52.70% and 19.00%, respectively, of the total variance in the rapeseed PCFs. Specifically, we observed positive relationships between PCF and SOC, soil clay proportion and altitude, while PCF was negatively correlated with per capita GDP, soil conductivity (PH), rapeseed yield, machinery and the soil-sand proportion. In addition, the weighted average PCF values from various regions did not exhibit a scattered distribution pattern, indicating that the PCFs exhibited a high degree of heterogeneity on the Chengdu Plain.

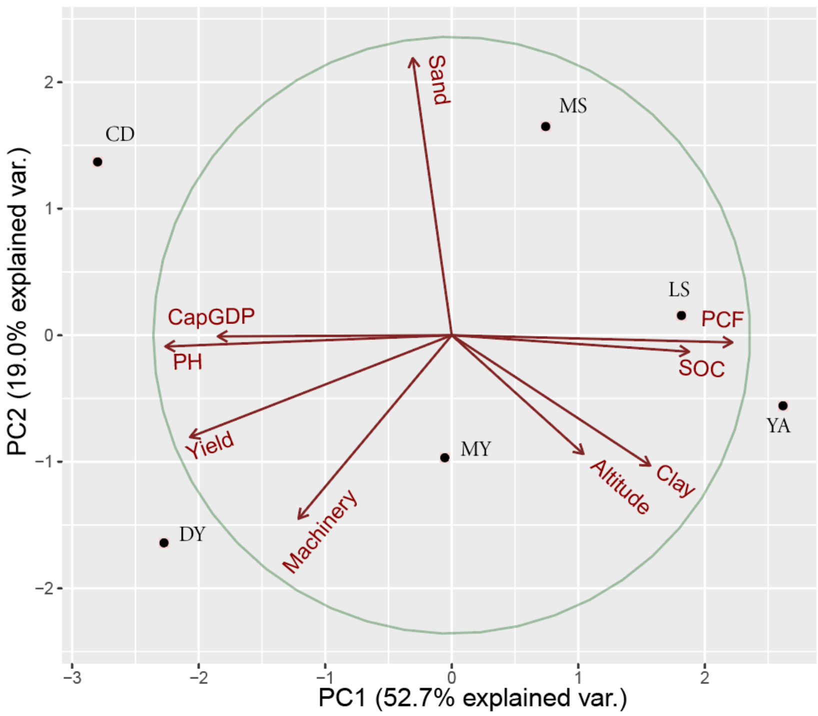

Note: PC1 and PC2 represent the first and second principal components, respectively. The explanatory variables are CapGDP, PH, yield, machinery, altitude, clay, SOC and sand. The response variable was the PCF of rapeseed.

Figure 7. Principal component analysis of selected variables and PCF.

4. Discussion

4.1 The novelty of the current study and implications for crop carbon footprint evaluation

Some studies have attempted to link GIS with LCA to explore spatial-temporal patterns of carbon footprints in bioenergy (O'Keeffe et al., 2016a; O'Keeffe et al., 2016b; Yang et al., 2022), biodiversity (Di Fulvio et al., 2019) and other relevant studies (Loiseau et al., 2018). However, studies using RS to extract crop information for improving LCA-based CF evaluation are still scarce. The novelty of our study is that it is the first to introduce RS together with GIS into rapeseed CF assessment. The motivation behind this approach is that the key information of crops used for CF evaluation, such as crop distribution, phenology and yield information, obtained from RS has the advantages of revealing fine spatial patterns and saving costs when compared to traditional approaches (O'Keeffe et al., 2016b). This study showed that RS can provide an acceptable basemap of rapeseed distribution, as illustrated in Figure 4. We did not use RS-based yield estimation for improving the PCF of rapeseed, which is beyond the scope of the current study. Nevertheless, there are already successful RS-based case studies in which rapeseed yield prediction models were developed using linear (Sulik and Long, 2015; Fang et al., 2016; Kern et al., 2018) and nonlinear models (Fan et al., 2021; Rajković et al., 2021), which can make good use of rapeseed phenological patterns and vegetation indices, e.g., NDVI and NDYI, for yield estimation. This study can serve as a good foundation for future crop CF assessment improvements. In summary, we encourage future studies to exploit RS and GIS to capture the spatial-temporal heterogeneity of rapeseed CFs at finer resolutions. This approach can also be applied to other crops or different regions with updated local information.

4.2 Spatial heterogeneity in rapeseed carbon footprints and its driving forces

The evaluation of rapeseed production and its byproducts, e.g., biodiesel and associated GHG emissions, currently attracts the attention of scholars worldwide. We observed large spatial heterogeneities in the rapeseed-associated CFs in the present study, as presented in Figure 6 and Appendix, Figure S.4b, which are generally in line with the findings of other studies. Due to the differences in rapeseed types, cultivation modes, hydrothermal conditions and management practices, the FCF of rapeseed is approximately 308-6,200 kg CO_2 eq ha^{-1} (Brandao et al., 2010; Forleo et al., 2018; Kesieme et al., 2019), and that of PCF is approximately 794.00 - 5,904.00 kg CO_2-eq

t^{-1} worldwide (Iriarte et al., 2010; Palmieri et al., 2014; Bieńkowski et al., 2015; Forleo et al., 2018), suggesting significant spatiotemporal heterogeneities. In addition, during the whole process of rapeseed cultivation, transportation, refining and biodiesel extraction, rapeseed cultivation has a global warming potential ranging from 53.30 - 79.00% (González-García et al., 2013; Yang et al., 2022). During this process, the consumption of N fertilizer, pesticides and agricultural machinery fuel are the main sources of carbon emissions (Wu et al., 2021). As the second largest consumer of rapeseed oil in the world, China's energy utilization does not comply with the basic national policy of food security, resulting in a delay in research on the CF of rapeseed. However, in recent years, a growing body of literature has been published on this topic. Ji et al. (2021) analysed the spatial distribution pattern of rapeseed growth in China on a provincial basis and reported that the CF value of Chinese rapeseed plants was approximately 2,117.05 kg CO_2-eq ha^{-1} (1021.63 kg CO_2-eq t^{-1}). The direct carbon emission source is rapeseed cultivation, while indirect emissions mainly originate from fertilizer processing and manufacturing. Bai et al. (2021) conducted a life cycle-based CF analysis for major oil crops in China and reported that the CF of rapeseed oil was approximately 3,354.55 kg CO_2-eq t^{-1}. Guo et al. (2022) conducted province-level analysis and reported that the rapeseed FCP and PCF in Sichuan Province were 2122 kg CO_2-eq ha^{-1} and 1014 kg CO_2-eq t^{-1}, respectively.

With respect to the influencing factors, a positive relationship between PCF and agricultural materials was observed, while PCF was negatively related to rapeseed yield (Guo et al., 2022). In addition, a study of the main grains (rice, wheat and maize) in China reported that 11 variables had significant impacts on the PCF: longitude, topsoil conductivity, latitude, topsoil organic carbon, population per land area, topsoil silt fraction, proportion of mechanical operation, total fertilizer consumption, topsoil sand fraction, and per unit area yield. Each factor displays a positive or negative relationship with a specific crop type (Tian et al., 2021). Consistent with other studies, our study highlighted the importance of SOC in rapeseed PCF estimation (Figure 7). SOC sequestration plays a fundamental role in mitigating CF under long-term fertilization, and SOC sequestration can change over time and vary substantially among cropping systems (Gan et al., 2012; Saeed et al., 2022). The offset of GHG emissions from SOC change can decrease the overall emissions in crop systems and provide a soil C sink in agricultural systems (Gan et al., 2012; Xue et al., 2014; Liu et al., 2018; Wang et al., 2021). Against this background, the third national soil condition census from 2022 to 2025 in China (PRC, 2022) can provide valuable inputs, such as comprehensive information on soil properties and geographic locations, for crop CF estimation soon.

4.3 Limitations and uncertainties of the current study

The present study on the estimation of rapeseed CF has several limitations. First, accurate detection of the flowering period is the foundation of RS-based rapeseed mapping. Therefore, the availability of flowering images directly affects the effectiveness of rapeseed monitoring. Due to the monsoon climate characteristics of most rapeseed planting areas in China, images of flowering periods are not always available. In addition, small patches of rapeseed fields and complex agronomic management can cause uncertainty during image classification. Thus, sufficient ground truth points are needed to guarantee map classification accuracy. Apart from the abovementioned aspects, the rapeseed yield information varies by publication source, data collection time and collection approach. We believe that if the rapeseed yield can obtain a relatively finer spatial-temporal resolution, the PCF might be closer to real-world conditions. For example, we can clearly observe the improvement of rapeseed PCF estimation with support of various resolutions of rapeseed yield information. The classic agricultural-statistic-based approach is shown in Figure 6b, the RS-mapping approach is shown in Figure 6d, and the surveyed yield information is shown in Appendix, Figure S.4b. Certainly, depending on the orientation of different studies, this is not a golden-rule to suggest a finer resolution of crop yield collection. Here, we recommend this approach under the context of regional studies. In addition to the abovementioned uncertainties and limitations, the present study could still provide a useful reference for identifying GHG emission hotspots and guiding effective agricultural carbon reduction policies.

5. Conclusion

In this study, we developed a novel rapeseed carbon footprint evaluation approach by integrating a fine-resolution rapeseed map developed by RS techniques. This method shows its superiority over previous GIS-LCA integrated studies in taking rapeseed physiological growth and phenological stages into account. Large variations in the rapeseed FCF and PCF are observed in the studied area. Additionally, the surveyed regional rapeseed yield map plays an important role in improving PCF estimation both quantitively and spatially. Furthermore, the current study revealed positive relationships between PCF and SOC, soil clay proportion and altitude, while PCF was negatively correlated with per capita GDP, soil conductivity, rapeseed yield, machinery and soil sand proportion. This implies the significant role of soil properties and SOC in influencing crop PCF. The findings of our study call attention to exploring the potential of remote sensing in crop yield estimation, which is considered a crucial parameter for PCF assessment. The integration of RS and GIS can capture spatial-temporal heterogeneity and thus provide dynamic monitoring of rapeseed carbon footprint evaluation. The method itself is transferable to other crops and regions with updated local information.

References

Ashourloo, D., H. S. Shahrabi, M. Azadbakht, H. Aghighi, H. Nematollahi, A. Alimohammadi, and A. A. Matkan. 2019. Automatic Canola Mapping Using Time Series of Sentinel 2 Images ISPRS. Journal of Photogrammetry and Remote Sensing 156:63–76. https://doi.org/10.1016/j.isprsjprs.2019.08.007.

Bai, Y. Y., Y. J. Zhai, C. X. Ji, T. Z. Zhang, W. Chen, X. X. Shen, and J. L. Hong. 2021. Environmental sustainability challenges of China's edible vegetable oil industry: From farm to factory. Resources, Conservation and Recycling 170:105606. https://doi.org/10.1016/j.resconrec.2021.105606.

Bieńkowski, J. F., R. Dąbrowicz, M. Holka, and J. Jankowiak. 2015. Carbon footprint ofrapeseed in conventional farming: case study of large-sized farms in Wielkopolskaregion (Poland). Asian Journal of Applied Science and Engineering 4:191-200.

Boettcher, R., A. L. Zappe, P. F. de Oliveira, Ê. L. Machado, A. L. Lawisch-Rodriguez, and D. A. Rodriguez-Lopez. 2020. Carbon Footprint of Agricultural Production and Processing of Tobacco (Nicotiana Tabacum) in Southern Brazil. Environmental Technology & Innovation 18. https://doi.org/10.1016/j.eti.2020.100625.

Brandao, M., R. Clift, L. Mila i Canals, and L. Basson. 2010. A life-cycle approach to characterising environmental and economic impacts of multifunctional landuse systems: an integrated assessment in the UK. Sustainability 2:3747-3776. https://doi.org/10.3390/su2123747.

Chen, X. H., C. C. Ma, H. M. Zhou, Y. Liu, X. M. Huang, M. K. Wang, Y. Y. Cai, D. Su, M. A. Muneer, M. C. Guo, X. J. Chen, Y. Zhou, Y. Hou, W. F. Cong, J. X. Guo, W. Q. Ma, W. F. Zhang, Z. L. Cui, L. Q. Wu, S. G. Zhou, and F. S. Zhang. 2021. Identifying the main crops and key factors determining the carbon footprint of crop production in China, 2001-2018. Resources, Conservation and Recycling 172:105661. https://doi.org/10.1016/j.resconrec.2021.105661.

Chen, X. P., Z. L. Cui, M. S. Fan, P. Vitousek, M. Zhao, W. Q. Ma, Z. L. Wang, W. J. Zhang, X. Y. Yan, J. C. Yang, X. P. Deng, Q. Gao, Q. Zhang, S. W. Guo, J. Ren, S. Q. Li, Y. L. Ye, Z. H. Wang, J. L. Huang, Q. Y. Tang, Y. X. Sun, X. L. Peng, J. W. Zhang, M. R. He, Y. J. Zhu, J. Q. Xue, G. L. Wang, L. Wu, N. An, L. Q. Wu, L. Ma, W. F. Zhang, and Z. F. Suo. 2014. Producing more grain with lower environmental costs. Nature 514:486–489. https://doi.org/10.1038/nature13609.

Di Fulvio, F., N. Forsell, A. Korosuo, M. Obersteiner, and S. Hellweg. 2019. Spatially explicit LCA analysis of biodiversity losses due to different bioenergy policies in the European Union. Science of the Total Environment 651:1505-1516. https://doi.org/10.1016/j.scitotenv.2018.08.419

Escobara, N., E. J. Tizado, E. K. H. J. zu Ermgassen, P. Löfgren, J. Börner, and J. Giodar. 2020. Spatially-explicit footprints of agricultural commodities: Mapping carbon emissions embodied in Brazil's soy exports. Global Environmental Change 62:102067. https://doi.org/10.1016/j.gloenvcha.2020.102067.

Fan, H., S. Liu, J. Li, L. Li, L. Dang, T. Ren, and J. Lu. 2021. Early prediction of the seed yield in winter oilseed rape based on the near-infrared reflectance of vegetation (NIRv). Computers and Electronics in Agriculture 186:106166. https://doi.org/10.1016/j.compag.2021.106166.

Fang, S., W. Tang, Y. Peng, Y. Gong, and K. Liu. 2016. Remote estimation of vegetation fraction and flower fraction in oilseed rape with unmanned aerial vehicle data. Remote Sensing 8:416. https://doi.org/10.3390/rs8050416.

Feng, X. M., T. Sun, J. R. Guo, H. G. Cai, C. R. Qian, Y. B. Hao, Y. Yu, A. X. Deng, Z. W. Song, and W. J. Zhang. 2023. Climate-smart agriculture practice promotes sustainable maize production in northeastern China: Higher grain yield while less carbon footprint. Field Crops Research 302:109108. https://doi.org/10.1016/j.fcr.2023.109108.

Finnveden, G. 2000. On the Limitations of Life Cycle Assessment and Environmental Systems Analysis Tools in General. The International Journal of Life Cycle Assessment 5:229-238. https://doi.org/10.1007/BF02979365.

Forleo, M. B., i. N. Palmier, A. Suardi, D. Coaloa, and L. Pari. 2018. The Eco-Efficiency of Rapeseed and Sunflower Cultivation in Italy. Joining Environmental and Economic Assessment. Journal of Cleaner Production 172:3138–3153. https://doi.org/10.1016/j.jclepro.2017.11.094.

Gan, Y., C. Liang, C. A. Campbell, R. P. Zentner, R. L. Lemke, H. Wang, and C. Yang. 2012. Carbon footprint of spring wheat in response to fallow frequency and soil carbon changes over 25 years on the semiarid Canadian prairie. European Journal of Agronomy 43:175–184. https://doi.org/10.1016/j.eja.2012.07.004.

Gasol, C. M., X. Gabarrell, M. Rigola, S. González-García, and J. Rieradevall. 2011. Environmental assessment: (LCA) and spatial modelling (GIS) of energy crop implementation on local scale. Biomass and Bioenergy 35:2975-2985. https://doi.org/10.1016/j.biombioe.2011.03.041.

González-García, S., D. García-Rey, and A. Hospido. 2013. Environmental life cycle assessment for Rapeseed-derived biodiesel. The International Journal of Life Cycle Assessment 18:61-76. https://doi.org/10.1007/s11367-012-0444-5.

Guo, C. Y., Z. H. Bai, X. Z. Wang, W. S. Zhang, X. J. Chen, P. Lakshmanan, L. Ma, J. W. Lu, B. Liu, X. J. Shi, and X. P. Chen. 2022. Spatio-temporal assessment of greenhouse gas emission from rapeseed production in China by coupling nutrient flows model with LCA approach. Food and Energy Security 11:e398. https://doi.org/10.1002/fes3.398.

Han, J., Z. Zhang, Y. Luo, J. Cao, and Z. Li. 2021a. The Rapeseed Map10 Database: Annual Maps of Rapeseed at a Spatial Resolution of 10 m Based on Multi-Source Data. Earth System Science Data 13:2857–2874. https://doi.org/10.5194/essd-13-2857-2021.

Han, J. C., Z. Zhang, Y. C. Luo, J. Cao, L. L. Zhang, J. Zhang, and Z. Y. Li. 2021b. The Rapeseed Map10 database: annual maps of rapeseed at a spatial resolution of 10 m based on multi-source data. Earth System Science Data 13:2857-2874. https://doi.org/10.5194/essd-13-2857-2021.

Haung, J. X., Y. Q. Chen, J. Pan, W. R. Liu, G. L. Yang, X. P. Xiao, H. B. Zheng, W. G. Tang, H. M. Tang, and L. J. Zhou. 2019. Carbon footprint of different agricultural systems in China estimated by different evaluation metrics. Journal of Cleaner Production 225:939-948. https://doi.org/10.1016/j.jclepro.2019.04.044.

Hellweg, S., and I. C. L. Milà. 2014. Emerging Approaches, Challenges and Opportunities in Life Cycle Assessment. Science 344:1109-1113. https://doi. 10.1126/science.1248361.

IPCC. 2006. 2006 IPCC Guidelines for National Greenhouse Gas Inventories.*in* S. Eggelston, L. Buendia, K. Miwa, T. Ngara, and K. Tanabe, editors.

IPCC. 2014. Climate change 2014: mitigation of climate change. contribution of working group III to the fifth assessment report of the intergovernmental panel

on climate change. United Kingdom and New York.
IPCC. 2019. N2O emissions from managed soils, and CO2 emssions from lime and urea application In: 2019 refinement to the 2006 IPCC guidelines for national greenhouse gas inventories (Chapter 11). United Kingdom and New York.
Iriarte, A., J. Rieradevall, and X. Gabarrell. 2010. Life cycle assessment of sunflower and rapeseed as energy crops under Chilean conditions. Journal of Cleaner Production 18:336-345. https://doi.org/10.1016/j.jclepro.2009.11.004.
ISO14067. 2013. ISO/TS 14067:2013 Greenhouse gases - Carbon footprint of products - Requirements and guidelines for quantification and communication
Ji, C., Y. Zhai, T. Zhang, X. Shen, Y. Bai, and J. Hong. 2021. Carbon, energy and water footprints analysis of rapeseed oil production: a case study in China. Journal of Environmental Management 287:112359. https://doi.org/10.1016/j.jenvman.2021.112359.
Kern, A., Z. Barcza, H. Marjanović, T. Árendás, N. Fodor, P. Bónis, P. Bognár, and J. Lichtenberger. 2018. Statistical modelling of crop yield in central Europe using climate data and remote sensing vegetation indices. Agricultural and Forest Meteorology 260-261:300-320. https://doi.org/10.1016/j.agrformet.2018.06.009.
Kesieme, U., K. Pazouki, A. Murphy, and A. Chrysanthou. 2019. Attributional Life Cycle Assessment of Biofuels for Shipping: Addressing Alternative Geographical Locations and Cultivation Systems. Journal of Environmental Management 235:96-104. https://doi.org/10.1016/j.jenvman.2019.01.036.
Liu, W., G. Zhang, X. Wang, F. Lu, and Z. Ouyang. 2018. Carbon footprint of main crop production in China: magnitude, spatial-temporal pattern and attribution. Science of the Total Environment 645:1296–1308. https://doi.org/10.1016/j.scitotenv.2018.07.104.
Liu, Y. Z., W. Y. Gu, B. B. Liu, C. Zhang, C. Wang, Y. Yang, and M. H. Zhuang. 2022. Closing Greenhouse Gas Emission Gaps of Staple Crops in China. Environmental Science & Technology 56:9302-9311. https://doi.org/10.1021/acs.est.2c01978
Loiseau, E., L. Aissani, S. Le Féon, F. Laurent, J. Cerceau, S. Sala, and P. Roux. 2018. Territorial Life Cycle Assessment (LCA): What exactly is it about? A proposal towards using a common terminology and a research agenda. Journal of Cleaner Production 176:474-485. https://doi.org/10.1016/j.jclepro.2017.12.169.
Medel-Jiménez, F., T. Krexner, A. Gronauer, and I. Kral. 2024. Life cycle assessment of four different precision agriculture technologies and comparison with a conventional scheme. Journal of Cleaner Production 434:140198. https://doi.org/10.1016/j.jclepro.2023.140198.
Medel-Jiménez, F., G. Piringer, A. Gronauer, N. Barta, R. W. Neugschwandtner, T. Krexner, and I. Kral. 2022. Modelling soil emissions and precision agriculture in fertilization life cycle assessment - A case study of wheat production in Austria. Journal of Cleaner Production 380:134841. https://doi.org/10.1016/j.jclepro.2022.134841.
Menegat, S., A. Ledo, and R. Tirado. 2022. Greenhouse gas emissions from global production and use of nitrogen synthetic fertilisers in agriculture. Scientific Report 12:14490. https://doi.org/10.1038/s41598-022-18773-w
Meng, S., Y. Zhong, C. Luo, X. Hu, and S. Huang. 2020. Optimal temporal window selection for winter wheat and rapeseed mapping with Sentinel-2 Images: a case study of Zhongxiang in China. Remote Sensing 12:226. https://doi.org/10.3390/rs12020226.

O'Keeffe, S., S. Wochele-Marx, and D. Thrän. 2016a. RELCA: a regional life cycle inventory for assessing bioenergy systems within a region. Energy, Sustainability and Society 6:1-19. https://doi.org/10.1186/s13705-016-0078-8.

O'Keeffe, S., S. Wochele-Marx, and D. Thrän. 2016b. RELCA: a regional life cycle inventory for assessing bioenergy systems within a region. Energy, Sustainability and Society 6:12. https://doi.org/10.1186/s13705-016-0078-8.

Palmieri, N., M. B. Forleo, A. Suardi, D. Coaloa, and L. Pari. 2014. Rapeseed for energy production: Environmental impacts and cultivation methods. Biomass and Bioenergy 69:1-11. https://doi.org/10.1016/j.biombioe.2014.07.001.

Peng, W. L., R. Wang, X. L. Chen, A. H. Liu, and W. D. Zheng. 2023. Effects of varied rapeseed varieties and cultivation measures on harvest index. Scientia Agricultura Sinica 56:3331-3346. https://doi.org/10.3864/j.issn.0578-1752.2023.17.008.

PRC. 2022. Notice of the State Council on carrying out the Third National Soil Census. State Council, PRC.

Rajković, D., A. M. Jeromela, L. Pezo, B. Lončar, F. Zanetti, A. Monti, and A. Kondić-Špika. 2021. Yield and quality prediction of winter rapeseed—artificial neural network and random forest models. Agronomy 12:58. https://doi.org/10.3390/agronomy12010058.

Reap, J., F. Roman, S. Duncan, and B. Bras. 2008. A survey of unresolved problems in life cycle assessment. The International Journal of Life Cycle Assessment 13:374-388. https://doi.org/10.1007/s11367-008-0008-x.

Rosenzweig, C., C. Mbow, L. G. Barioni, T. G. Benton, M. Herrero, M. Krishnapillai, E. T. Liwenga, P. Pradhan, M. G. Rivera-Ferre, T. Sapkota, F. N. Tubiello, Y. Xu, E. Mencos Contreras, and J. Portugal-Pereira. 2020. Climate change responses benefit from a global food system approach. Nature Food 1:94-97. https://doi.org/10.1038/s43016-020-0031-z.

Saeed, Q., A. Zhang, A. Mustafa, B. H. Sun, S. L. Zhang, and X. Y. Yang. 2022. Effect of longterm fertilization on greenhouse gas emissions and carbon footprints in northwest China: A field scale investigation using wheat-maize-fallow rotation cycles. Journal of Cleaner Production 332:130075. https://doi.org/10.1016/j.jclepro.2021.130075.

Sulik, J. J., and D. S. Long. 2015. Spectral indices for yellow canola flowers. International Journal of Remote Sensing 36:2751-2765. https://doi.org/10.1080/01431161.2015.1047994.

Tabatabaie, S. M. H., H. Tahami, and G. S. Murthy. 2018. A regional life cycle assessment and economic analysis of camelina biodiesel production in the Pacific Northwestern US. Journal of Cleaner Production 172:2389-2400. https://doi.org/10.1016/j.jclepro.2017.11.172.

Tao, J., W. Wu, W. Liu, and M. Xu. 2020. Exploring the Spatio-Temporal Dynamics of Winter Rape on the Middle Reaches of Yangtze River Valley Using Time-Series MODIS Data. Sustainability 12:466. https://doi.org/10.3390/su12020466.

Tao, J. B., W. B. Liu, W. X. Tan, X. B. Kong, and M. Xu. 2019. Fusing multi-source data to map spatio-temporal dynamics of winter rape on the Jianghan Plain and Dongting Lake Plain, China. Journal of Integrative Agriculture 10:2393-2407. https://doi.org/10.1016/S2095-3119(19)62577-3.

Tian, P. P., D. Li, H. W. Lu, S. S. Feng, and Q. W. Nie. 2021. Trends, distribution, and impact factors of carbon footprints of main grains production in China. Journal of Cleaner Production 278:123347.

https://doi.org/10.1016/j.jclepro.2020.123347.
Wang, L. L., L. L. Li, J. H. Xie, Z. Z. Luo, R. Z. Zhang, L. Q. Cai, J. A. Coulter, and J. A. Palta. 2021. Managing the trade-offs among yield, economic benefits and carbon and nitrogen footprints of wheat cropping in a semi-arid region of China. Science of the Total Environment 768:145280. https://doi.org/10.1016/j.scitotenv.2021.145280.
Wang, X. L., Y. Chen, X. W. Chen, R. R. He, Y. S. Guan, Y. W. Gu, and Y. Chen. 2019. Crop production pushes up greenhouse gases emissions in China: evidence from carbon footprint analysis based on national statistics data. Sustainability 11:4931. https://doi.org/10.3390/su11184931.
Wu, H., G. K. MacDonald, J. N. Galloway, L. Zhang, L. Gao, L. Yang, J. Yang, X. Li, H. Li, and T. Yang. 2021. The influence of crop and chemical fertilizer combinations on greenhouse gas emissions: a partial life cycle assessment of fertilizer production and use in China. Resources, Conservation and Recycling 168:105303. https://doi.org/10.1016/j.resconrec.2020.105303.
Xue, J. F., S. L. Liu, Z. D. Chen, F. Chen, R. Lal, H. M. Tang, and H. L. Zhang. 2014. Assessment of carbon sustainability under different tillage systems in a double rice cropping system in Southern China. International Journal of Life Cycle Assessment 19:1581–1592. https://doi.org/10.1007/s11367-014-0768-4.
Yang, X. Q., Y. Liu, A. Bezama, and D. Thrän. 2022. Two birds with one stone: a combined environmental and economic performance assessment of rapeseed-based biodiesel production. GCB Bioenergy 14:215-241. https://doi.org/10.1111/gcbb.12913.
Zang, Y. Z., Y. A. Qiu, X. H. Chen, J. Chen, W. Yang, Y. F. Liu, L. K. Peng, M. G. Shen, and X. Cao. 2023. Mapping rapeseed in China during 2017-2021 using Sentinel data: an automated approach integrating rule-based sample generation and a one-class classifier (RSG-OC). GIScience & Remote Sensing 60:2163576. https://doi.org/10.1080/15481603.2022.2163576.
Zeng, L., B. D. Wardlow, D. Xiang, S. Hu, and D. Li. 2020. A review of vegetation phenological metrics extraction using time-series, multispectral satellite data. Remote Sensing of Environment 237:111511. https://doi.org/10.1016/j.rse.2019.111511.
Zhang, H. Y., W. B. Liu, and L. P. Zhang. 2022. Seamless and automated rapeseed mapping for large cloudy regions using time-series optical satellite imagery. ISPRS Journal of Photogrammetry and Remote Sensing 184:45-62. https://doi.org/10.1016/j.isprsjprs.2021.12.001.
Zhang, Q., X. T. Ju, and F. S. Zhang. 2010. Re-estimation of direct nitrous oxide emission from agricultural soils of China via revised IPCC2006 guideline method. Chinese Journal of Eco-Agriculture 18:7-13. https://doi.org/10.3724/SP.J.1011.2010.00007.
Zhang, W. F., Z. X. Dou, P. He, X. T. Ju, D. Powlson, D. Chadwick, D. Norse, Y. L. Lu, Y. Zhang, L. Wu, X. P. Chen, K. G. Cassman, and F. S. Zhang. 2013. New technologies reduce greenhouse gas emissions from nitrogenous fertilizer in China. PNAS 110:8375–8380. https://doi.org/10.1073/pnas.1210447110.
Zhang, Y. J., H. S. Niu, and Q. Yu. 2021. Impacts of climate change and increasing carbon dioxide levels on yield changes of major crops in suitable planting areas in China by the 2050s. Ecological Indicators 125:107588. https://doi.org/10.1016/j.ecolind.2021.107588.